Creep of aromatic polyamide fibres*

R. H. Ericksen
Sandia National Laboratories, Albuquerque, New Mexico 87185, USA
(Received 27 March 1984)

Creep of Kevlar 29, Kevlar 49 and PRD 49-III fibres was investigated. The fibres exhibited transient creep and the strain–time relationship was represented by a logarithmic time law. The creep strain recovered with time when the load was removed. Upon reloading to the same creep stress the strain–time relationship was again logarithmic but the creep rate was reduced. Modulus measurements were made during the creep test and these showed that the modulus increased with time. This result indicated a crystallite rotation mechanism which could account for the experimentally observed creep strain. Creep in PRD 49-III fibres exhibited a small temperature dependence over the temperature range 20°C to 150°C. The apparent creep activation energy was consistent with the range of values reported for hydrogen bonding. This suggests one possible creep mechanism in which the combined action of stress and thermal activation causes rearrangement of intercrystalline bonds in the crystallite boundaries resulting in boundary creep. Boundary creep allows crystallite rotation which produces the macroscopic creep strain. Boundary creep is discussed in terms of the fibre morphology and a model of delayed elasticity.

(Keywords: fibre creep; polyamide fibres; crystallite rotation; creep model; recovery; modulus)

INTRODUCTION

The interest in synthetic aromatic polyamides (aramids) has increased with the commercial availability of the high-strength, high-modulus fibre Kevlar. Symposia reports and reviews[1–15] now summarize a large number of papers in the literature concerning Kevlar and related fibres. Because of its unique combination of physical and mechanical properties Kevlar has found many applications in textiles and in reinforced composites. In many cases the high strength and high modulus of Kevlar are primary factors which dictate its use. Studies have been reported concerning stress–strain, fatigue, compressive and other strength-related properties[16–26]. In particular, the work of Northolt and van Aartsen[27], and Northolt[28] on the deformation mechanism of poly(*p*-phenylene terephthalamide), PPTA, fibres has provided a basis for understanding the mechanism of aromatic fibre deformation. It has been reported that the fibres are essentially 100% crystalline[9]. Northolt[28] has shown that the stress–strain curve for PPTA fibres is a result of elastic strain and irreversible rotation of the crystallites.

In the case of time-dependent deformation, the stress-rupture of Kevlar strands and composites has been investigated[29–31] but relatively little information is available concerning Kevlar fibre creep. Room temperature creep curves for Kevlar strands are reported in Dupont's Kevlar Data Manual[32]. Bunsell[18] has described a creep curve for a single Kevlar 49 fibre at 85% of the fibre breaking load, and some room temperature creep data for single fibres were reported as part of an earlier study of the creep of Kevlar/epoxy composites[33]. These data indicate that Kevlar fibres exhibit more creep than other commonly utilized high-performance composite reinforcements such as glass[34], boron[35] or graphite[36].

In some instances creep deformation could be a limiting factor in use of Kevlar composites, and information concerning the creep mechanism will be useful in understanding the origin of time-dependent failure. The present study was initiated to determine the creep behaviour of Kevlar fibres and to provide a basis for understanding the creep mechanism in terms of structural and morphological features of the fibres. Experiments were performed to evaluate the importance of crystallite rotation during creep. A mechanism is proposed in which boundary creep resulting from intercrystallite bond motion allows crystallite rotation which produces macroscopic creep.

EXPERIMENTAL

Material

Three types of fibres manufactured by E. I. Dupont Co., Wilmington, Delaware were investigated.*

(1) PRD 49-III from 4670 denier roving (Merge 6G045, Ball No. 112–3, Lot No. 11).

(2) Kevlar 49 from 195 denier yarn (Merge 6G015, Spinning POS 22R, LOT 284, DOFF 1050: Finishing POS 12, LOT 303, DOFF 0145).

(3) Kevlar 29 from 400 denier yarn (Merge 6F025).

The outside layers of yarn from each spool were discarded then lengths of yarn were removed as needed for sample preparation. Individual fibre samples were obtained by carefully separating one or more fibres from the

* This work performed at Sandia National Laboratories supported by the US Departmenr of Energy under contract DE-AC04-DP00789.

* Kevlar 29 and 49 fibres have been shown to be poly(*p*-phenylene terephthalamide), PPTA, (13,15). We believe our PRD 49-III fibers are the same polymer. Reference to PPTA fibres in this paper designates that the fibres have not been specifically cited as having been manufactured by Dupont.

0032-3861/85/050733-14$03.00

yarn. At the first indication of fibre interaction or entanglement a new piece of yarn was used. Between sampling, the spools of yarn were kept covered to avoid any degradation due to laboratory lighting.

CREEP TESTING

Two different types of test apparatus were used in this investigation. The first tests were carried out using a feedback loading system to provide constant load application. Strain was measured using an optical extensometer. Later, a new fibre test system was developed: this employed deadweight loading and an LVDT strain measuring system. The details of each apparatus are described below.

Feedback load control system

Load application was carried out using an Instron testing machine equipped with a hydraulic attachment and feedback load control system. A 50 g load cell was used and the load was held constant during the creep tests to within 1%. The fibres were gripped using conventional clothespin type fibre grips with aluminium foil inserts. No evidence of grip slippage was noted and when fibre failure was observed it was away from the grips.

Displacement was measured using an optical extensometer having a resolution of about 5×10^{-3} cm. Drops of epoxy were placed on the fibre test sample to define a 35 cm gauge length and to serve as reference markers for the displacement measurements. The crosshairs of the filar eyepieces in the optical extensometer were zeroed on the markers, and then the displacement of one mark relative to the other was monitored during the test. The two tracking eyepieces were mounted on an Invar bar to minimize drift caused by temperature fluctuations. The strain measurement sensitivity was largely limited by the ability of the operator to reproduce the position of the crosshair on the image of the epoxy marker. The strain reproducibility was about $\pm 2 \times 10^{-6}$.

An air oven was used for elevated temperature tests with the entire sample including grips located inside the oven. The specimen as back lighted and a quartz fibre was embedded in the drop of epoxy to provide an improved strain measuring target. The working distance of the extensometer was such that it could be positioned outside the oven. During all tests, both at room temperature and at elevated temperatures, a 0.25 g alignment preload was applied to the test specimen. Any creep which occurred under this preload was below the resolution of the strain measuring system.

Deadweight fibre tester

This system consisted of a deadweight load frame of 50 g capacity. Strain was measured with an LVDT, the core of which was part of the lower grip/weight tray assembly. The test specimen was mounted on a thin cardboard gasket and was bonded in place using room-temperature curing cellulose nitrate cement. Sample gauge lengths varied from 5 to 25 cm depending on the amount of strain expected during the test. The fibre and gasket were gripped in the test machine with two miniature alligator clips: then the cardboard mount was cut away. This left the fibre specimen hanging in the test fixture under the weight of the lower clamp, the linkage to the LVDT core, and the weight tray. Everything hanging below the specimen contributed to the alignment preload. The preload weight varied from 1 to 2.3 g depending on the particular load train configuration. The weights were applied by means of a motor driven elevator mechanism. A micrometer adjustment at the top of the load train provided for zeroing the core position of the LVDT and for calibration of the output. The LVDT output was digitized and stored on magnetic tape. Strain data was obtained during load application and during the initial part of the creep test at a rate of 40 points per second. Computer control of the acquisition system slowed the sampling rate according to a preset table so that as the creep rate slowed, fewer data points were obtained. The temperature of the apparatus was monitored and the strain data were corrected for thermal expansion of the test sample and load train.

An additional feature that was built into the loading mechanism allowed the main creep load to be applied in two steps. This also allowed a portion of the creep load to be removed and reapplied during a test. Using this technique, the sample modulus was measured as a function of creep strain.

For stress–strain tests, a LVDT load cell was mounted at the upper part of the load train. This introduced an additional compliance into the load train. A load *versus* load cell displacement curve was obtained by substituting a rigid aluminium strip for the test specimen. The cross section of the strip was sufficiently large so that its deformation was negligible. The data was then used to correct the apparent strain output for the load cell compliance. A rigid link from the LVDT displacement indicator to the mechanical drive of the weight elevator mechanism allowed direct mechanical loading of the sample. The loading rate could be varied between 0.8 and 40%/min.

RESULTS

Strain on loading: load–strain behaviour

The strain obtained on creep loading represents that portion of the load–strain curve obtained under the same deformation conditions. Load–strain curves for Kevlar 29 and 49 fibres are shown in *Figure 1* for: (a) loading to failure, $\bar{P}_f$, and (b) loading to $0.8\bar{P}_f$, followed by unloading

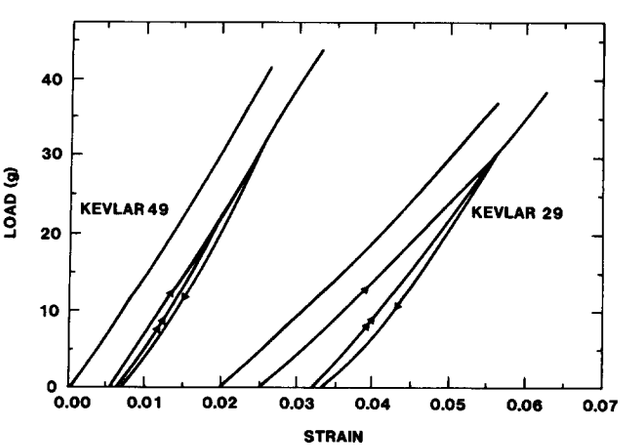

Figure 1 Load vs. strain curves for Kevlar 49 and Kevlar 29 single fibres. First curve for each fibre represents loading to failure. Second curve was loaded to 80% at the average failure load, unloaded, then reloaded to failure. Curves are offset along the strain axis for clarity

Table 1 Modulus (g/den) measured during various segments of stress-strain curve

	Initial loading 8%/min			Unloading 8%/min		Second loading 8%/min				Initial loading 0.8%/min	
Load range	5–30g	10–15g	20–25 g	5–30g	20–25g	5–30g	10–15g	20–25g	32.5–37.5g	10–15g	20–25g
Kevlar 49	1038	1008	1079	1172	1348	1133	1070	1173	1146	1011	1093
PRD 49–III	–	914	975	–	–	–	–	–	–	895	956
Kevlar 29	–	613	709	–	1156	–	–	1048	–	644	–

Averages of five tests

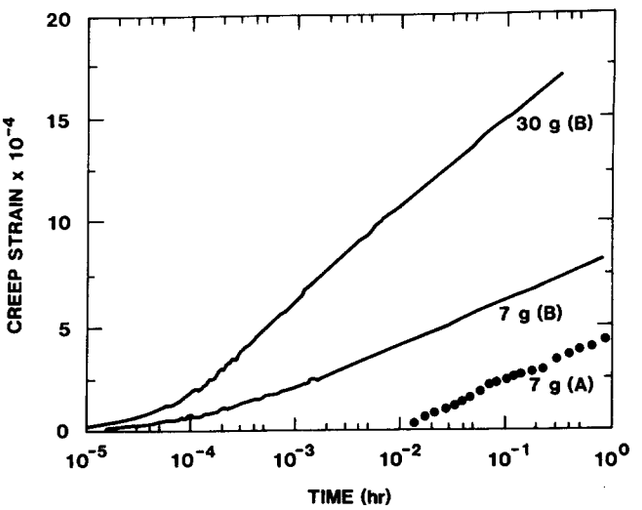

Figure 2 Room temperature creep curves for PRD 49-III single fibres. Curves at 7g were obtained using (A) optical and (B) LVDT strain measuring techniques

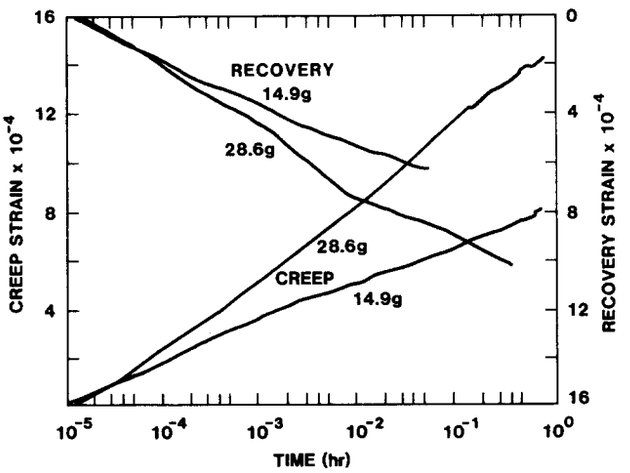

Figure 3 Room temperature creep and recovery curves for Kevlar 49 single fibres

and reloading to failure. Elastic modulus data are shown in *Table 1*. The stress–strain curve for Kevlar 49 was also representative of that for the PRD 49-III although the modulus of the PRD 49-III fibres was lower. The Kevlar 49 load–strain curve was nearly linear; however, some curvature was apparent on close examination. Initially, up to about 15 g load, the curve exhibited a slight concave upward curvature. For example, the average modulus of the Kevlar 49 fibres was measured to be 1008 g/den in the load range 10 to 15 g and 1029 g/den in the load range 20 to 25 g. Above 15 g the load–strain curve was linear until at loads above 40 g some of the fibre load–strain curves exhibited a slight downward curvature.

In the case of Kevlar 29 the load–strain curves exhibited the same general shape but the curvature was more pronounced. On initial loading average modulus values were 613 g/den in the range 10 to 15 g, and 709 g/den in the range 20 to 25 g. Hysteresis is apparent in the curves unloaded from 0.8 $\bar{P}_f$ with more observed for Kevlar 29 than for Kevlar 49. The second loading showed higher moduli than those exhibited over comparable load ranges of the first loading. These modulus values are shown in *Table 1*. At loads above those attained on the initial loading, the initial and second loading curves superimpose.

On unloading from 0.8 $\bar{P}_f$, the load strain curve also exhibited some curvature. The initial modulus on unloading was higher than any values obtained on either the first or the second loadings. The average modulus over the entire unloading curve was still higher than that obtained on the initial loading but similar to that obtained during the second loading.

CREEP

Kevlar 49 and PRD 49-III fibres: initial creep

Room temperature creep curves for the Kevlar 49 and PRD 49-III fibres exhibited transient creep. The creep rate decreased with time. In addition, the curves were approximately linear when the creep strain was plotted *versus* the logarithm of time for times exceeding about 10^{-4} h after the creep stress was applied. Examples of these logarithmic creep curves are shown in *Figures 2* and *3*. Some of the creep curves exhibited a slight amount of curvature. Others tested under the same conditions were very linear. There was no consistent trend in the direction of the curvature that was observed; in some cases it was positive and in others it was negative. As a result, the data will be treated as logarithmic within experimental uncertainty. Most of the creep tests were 1 to 20 h long and in a few cases the tests were carried out to 200 h. In cases where the loads were near the range where tensile failure was expected, creep failure terminated the test. There was no indication in any of the tests of a systematic departure from logarithmic creep. The intervals between strain measurements varied depending on the duration of the test, but in most cases in which failure was obtained, the data points were obtained within a few seconds of each other.

The results described above are based on data obtained using both test methods described in the experimental section. The two test methods were completely different. Creep curves obtained using each method are compared in *Figure 2*. Curve A shows data from the feedback load control system using an optical extensometer. Curve B was from the deadweight system with an LVDT strain measuring device. The curves are displaced because of the

time required to obtain the initial reading using the optical extensometer. In those cases this reading was taken as the initial strain. It is significant that the shape of the curves are the same. This provides evidence that the data represents material behaviour and not experimental errors such as slippage in the grips, electronic drift, or temperature variation. The data obtained using the LVDT output showed that logarithmic creep was obtained after about 10^{-4} h. There was a systematic upward curvature in all the curves for shorter times. This very short time data is subject to errors in defining the initial strain–time conditions and will not be considered in this study.

Logarithmic creep curves can be expressed simply as:

$$\varepsilon(t)_{t>t_0}=\varepsilon'(\sigma,\tau)+\alpha(\sigma,\tau)\mathrm{Log}_{10}t \qquad (1)$$

where $\varepsilon(t)$ is the creep strain*, ε' refers to the strain when $t=1$, t_0 is an arbitrary small positive number and $\alpha(\sigma,\tau)$ is a parameter which is independent of time but varies with load, temperature and environmental variables. It is particularly convenient to use this expression since the parameter α is the slope of the strain *versus* log time plot for constant load creep (strain per decade in time), i.e.

$$\alpha=\frac{\mathrm{d}\varepsilon}{\mathrm{dLog}_{10}t} \qquad (2)$$

and this parameter is related to the creep rate $\dot{\varepsilon}$ by

$$\dot{\varepsilon}=\frac{\alpha}{2.3t} \qquad (3)$$

This single parameter relationship between α and $\dot{\varepsilon}$ for logarithmic creep facilitates comparison of creep data and is used in this paper. It should be emphasized that even though α is constant for a given creep test, the creep rate continually decreases with time. The creep is always transient and no evidence of either a steady state creep component or a third stage was observed.

Since the creep curves are linear on the semi-log plots to relatively short times, the use of more rigorous expressions such as $\mathrm{Log}(a+bt)$[37] to describe logarithmic creep is not warranted.

Effect of load on initial creep

Logarithmic creep persists over the entire load range for Kevlar 49 and PRD 49-III fibres. When load is increased, the creep rate parameter, α, shows an increasing trend. There is scatter in the values of α from sample to sample when tests at the same load are compared. These are thought to arise from differences in fibre cross sectional area, changes in laboratory temperature and humidity (nominally 20°C–22°C and 20–40% r.h.), and variation in fibre morphology. A definite relationship between the scatter and any one of these variables has not been identified. The parameter α is plotted *versus* load, P, on logarithmic coordinates in *Figures 4* and *5*. A log–log plot was used because creep rate data in many materials exhibits a power law dependence on stress. Resolution of the details of the stress dependence was not attempted in this study.

* Only the creep strain is shown in the creep curves in this paper to allow curves at several load levels to be shown on the same plot. To obtain the total strain, the initial strain must be added to the creep strain.

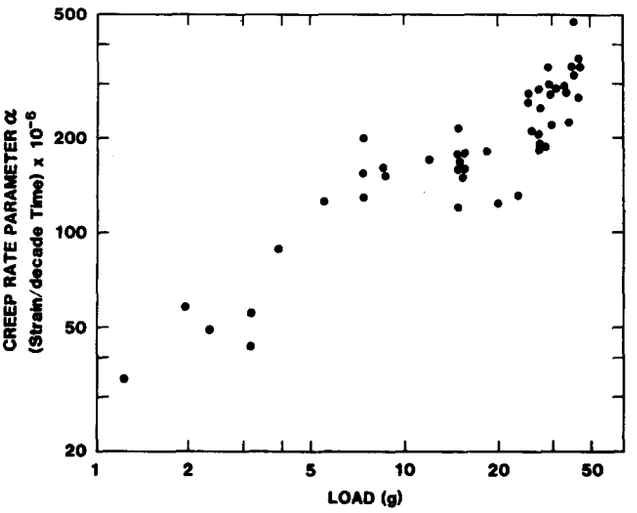

Figure 4 Log–log plot of creep rate parameter, *a*, *versus* load for PRD 49-III single fibres at room temperature

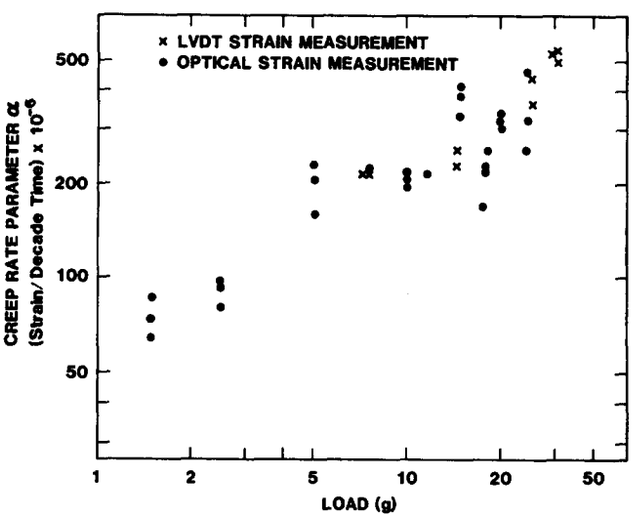

Figure 5 Log–log plot of creep rate parameter, *a*, *versus* load for Kevlar 49 single fibres at room temperture

Recovery following initial creep

When the load was removed (to the level imposed by the alignment pre-load) after creep, there was an instantaneous reduction in strain followed by a further reduction in strain with time. The time-dependent recovery curves for PRD 49-III and Kevlar 49 showed an initial approximately linear decrease in strain with log time. A set of creep and relaxation data are shown in *Figure 3*. When the duration of the recovery test exceeded that of the previous creep test, the recovery strain started to deviate from the linear semi-log plot and less recovery was obtained than expected from the initial part of the curve. This can be seen in the recovery curves in *Figure 6*. The absolute value of the slope of the initial recovery curves was slightly less than the slope of the preceding creep curves, 76% in the case of PRD-III and 83% for Kevlar 49. The slope of the initial recovery curves varies with the applied load in the same way as slope of the initial creep curve (compare *Figure 6* with *Figures 4* and *5*).

The amount of recovery strain over a time interval equal to that of the previous creep test averaged 73% of the creep strain in the case of PRD 49-III and 80% in the

case of Kevlar 49. These values did not depend on the magnitude of the creep load. The data is shown in *Table 2*.

Multiple creep/recovery cycling

An example of a multiple creep/recovery curve (only the time-dependent strain in each case) is shown in *Figure 7*. The slopes of the second creep curves were on the average only 60% of the initial values. This ratio appeared to be the same over the entire load range. Although the initial creep time was not systematically varied, there was no indication that its length influenced the slope of the subsequent creep curve. Likewise, the length of recovery time did not seem to influence the subsequent creep behaviour. In all instances, the recovery times were at least as long as the prior creep tests. In one test a fibre was taken through four creep/recovery cycles. These results are shown in *Table 3*. The first creep curve had the highest slope, those for subsequent curves were lower and all the same. All the recovery curves had about the same slopes.

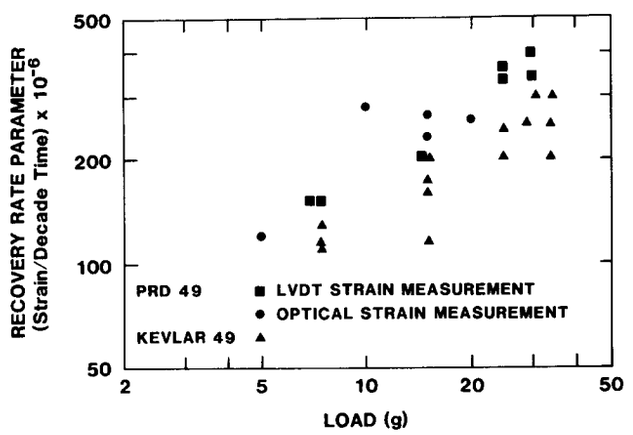

Figure 6 Recovery rate parameter (negative slope of logarithmic recovery curve) *versus* load for PRD 49-III and Kevlar 49 fibres at room temperature

Similar trends were seen in the modulus data from the loading and unloading curves. After the initial loading, both loading and unloading moduli did not change significantly.

Effect of temperature on initial creep

PRD 49-III fibres were creep tested at 65°C and 150°C for comparison with the room temperature data. Over this temperature range the fibres also exhibited logarithmic creep. Since there was no evidence of a deviation from this time law in any of the tests, all the data can be compared by plotting the creep rate parameter, α, *versus* load at each temperature. These curves are shown in *Figure 8*. The trend is for the creep rate to increase with temperature at low loads. As load is increased there are smaller increases in rate with temperature so that at the

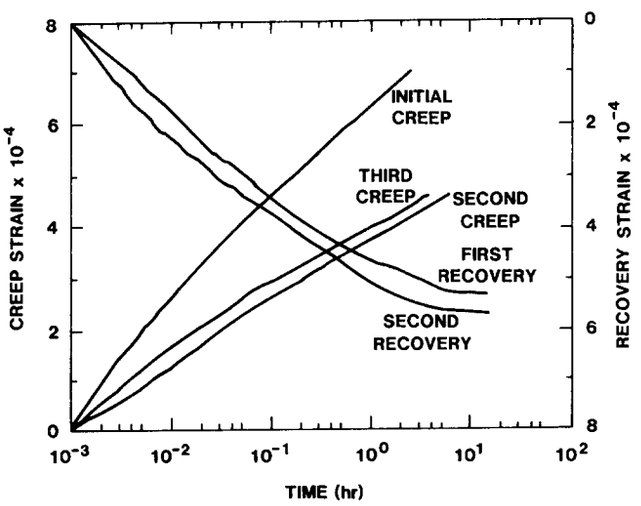

Figure 7 Repeated creep and recovery curves for Kevlar 49 fibres at room temperature. Creep load was 14.9g

Table 2 Percent of creep strain recovered (recovery time = creep time)

Kevlar 49		PRD-49		Kevlar 29	
Load (g)	Percent recovery	Load (g)	Percent recovery	Load (g)	Percent recovery
7.3	87	5	~100	7.1	51
7.3	59	7.1	73	7.4	63
14.9	79	7.1	>61	9.1	71
14.9	88	10	78	9.1	75
24.8	69	15	76	4.5	77
24.8	86	15	56	4.5	72
23.9	93	20	66	4.5	47
		24.8	83	4.7	76
		24.8	77	4.9	81
		30	76		
		30	59		

Table 3 Load/unload modules and creep/recovery curve slopes for multiple creep/recovery cycles on one fibre

	Modulus (g/den)		Slope (strain/decade time x 10^6)	
	Loading	Unloading	Creep	Recovery
Cycle 1	983	1051	275	200
Cycle 2	1044	1059	160	185
Cycle 3	1051	1066	155	230
Cycle 4	1051	1044	165	200

higher loads the creep rates are only slightly greater than those obtained at room temperature.

In the case of samples tested at 10 g, data were taken at additional temperatures. Since the creep rate parameter includes the temperature dependence, it is assumed to vary according to the Arrhenius equation. The 10 g data plotted as log α vs. $1/T$ is shown in *Figure 9*. This data indicates an apparent activation energy of 1.6 kcal/mole. Apparent activation energies were also estimated from the data at other loads. These varied from 4.4 kcal mol^{-1} at 1.5 g load to 1.5 kcal mol^{-1} at a load of 15 g.

In one elevated temperature test the load was removed following creep and the creep strain was observed to recover with time as in the case of the room temperature data. Upon reloading, logarithmic creep was observed and the rate was lower than that found during initial creep.

Modulus change during creep

Modulus data obtained during creep of Kevlar 49 at 24.6 g are shown in *Figure 10*. The data indicate that: (a) the moduli increased by about 6% during the initial 30 min of creep, (b) the moduli were higher than those obtained from the slope of the stress–strain curves in the 24–25 g load range, and (c) the moduli were about the same as those observed during unloading from 31.6 g in the stress–strain tests. One set of modulus data was

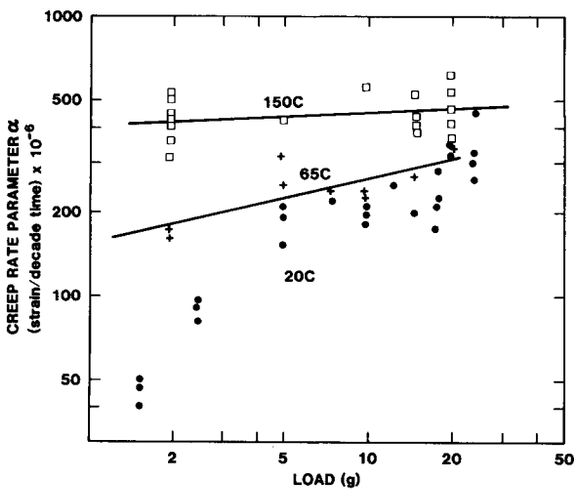

Figure 8 Effect of temperature on the creep rate *versus* behaviour of PRD 49-III fibres

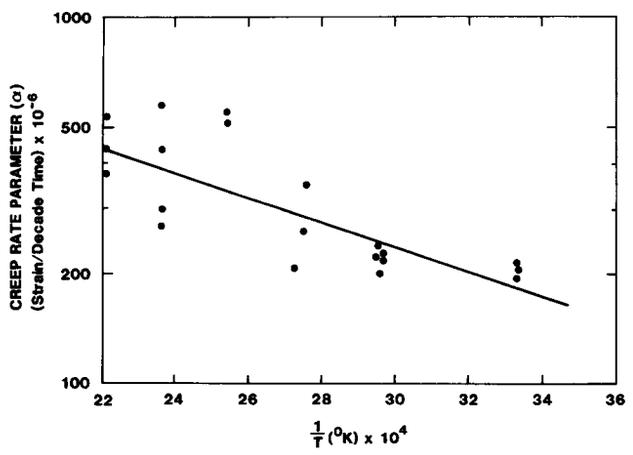

Figure 9 Arrhenius plot of PRD 49-III creep data

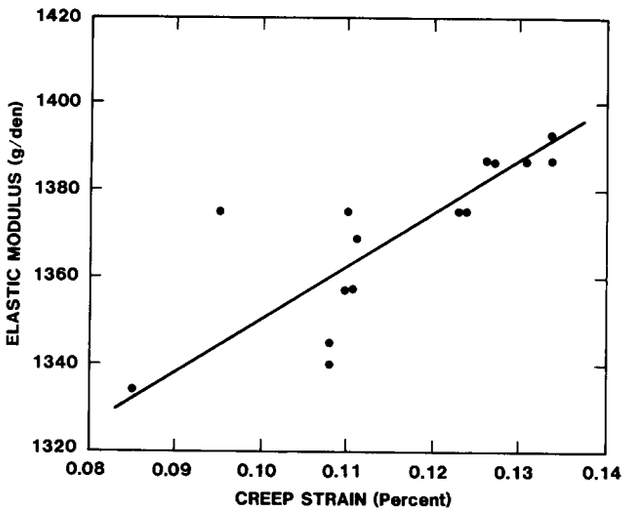

Figure 10 Elastic modulus measured during creep of a Kevlar 49 fibre at room temperature

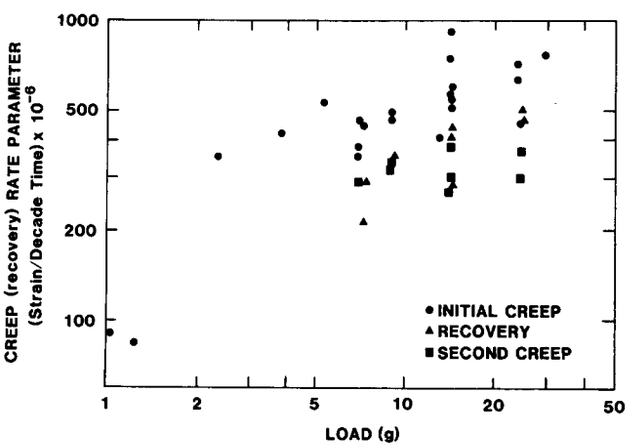

Figure 11 Creep and recovery rate parameter data for Kevlar 29 fibres during initial loading, recovery, and reloading at room temperature

obtained during the second creep loading of a Kevlar 49 fibre. This data demonstrated the same characteristics as described above.

Kevlar 29 fibre creep

As in the case of the PRD 49-III and Kevlar 49 fibres, the creep curves for Kevlar 29 fibres were also logarithmic. The main difference in behaviour among the different fibre types was found in the creep rate parameters. The effect of load on the creep rate and recovery parameters for the Kevlar 29 fibres is shown in *Figure 11*. The creep rates for Kevlar 29 were approximately three times higher than those of Kevlar 49 at creep loads above 5 g and were even higher at low loads.

For recovery times of 1 to 5 times that of the initial creep test about 70% of the creep strain recovered. The rate of recovery was similar, but somewhat lower, than that observed during creep. This can be seen by comparing the data in *Figure 11*. On reloading, the creep curves were also logarithmic and the creep rates were lower than those obtained initially as shown in *Figure 11*.

Modulus measurements during creep showed the same trends as observed for Kevlar 49 except that the rate of modulus increase with strain was higher in the case of Kevlar 29 by a factor of 2.3. This can be seen by comparing

the data in *Figure 12* with that in *Figure 10*. It should be noted that the modulus of Kevlar 29 measured during creep at 24.6 g had increased considerably over that measured during the load–strain or initial loading curves. On initial loading in the load–strain tests a modulus of 709 g/den was obtained in the 20 to 25 g range, while the first modulus measurements in the creep tests indicated moduli values exceeding 1200 g/den. These are to be compared with corresponding values of 1079 and 1330 g/-den for Kevlar 49.

DISCUSSION

Strain on loading: load–strain behaviour

The load–strain curves for the DuPont fibres of this investigation were obtained at a strain rate of 8% per min. They exhibited an initial concave upward slope, then a linear region, then a very slight downward curvature at high strains. This latter curvature was only apparent in the fibres that were in the upper part of the failure strength envelope. These observations hold for all the fibre types but the Kevlar 29 fibres exhibited these trends to a greater degree than the Kevlar 49 or PRD-III fibres. Ko[38] reported the same trends for the shape of Kevlar 49 stress–strain curves, but his modulus values were lower than those we measured. Northolt[28] reported the stress–strain curve for his PPTA fibres to be nearly linear at strain rates larger than 5% per min. His curves were slightly convex at large extensions. At low strain rates he reports a sigmoid-shaped stress–strain curve, particulary in the case of fibres with a relatively low initial modulus. The effect of strain rate on initial loading was not studied in our creep tests; however, three samples of each fibre type were loaded at a rate of 0.8% per min and no change in the shape of the load–strain curve could be observed. The modulus values compared favourably with those obtained at 8% per min and are summarized in *Table 1*. The static modulus for the highest modulus fibre tested by Northolt[28] was 826 g/den, a value slightly lower than that of the PRD 49-III fibres shown in *Table 1*. Residual deformations were reported by Northolt to be 0.14% for a strain of 1% to ~0.8% for a strain of 2.7%. In the present study the residual deformation was 0.23% for a strain of 1.85% for Kevlar 49, and 0.8% for a strain of 2.8% in the case of Kevlar 29. In summary, the differences in load or stress–strain behaviour between the fibres used in this study and those investigated by Northolt are not large. They most likely reflect different processing conditions in the fibre manufacture and possible differences in experimental procedures.

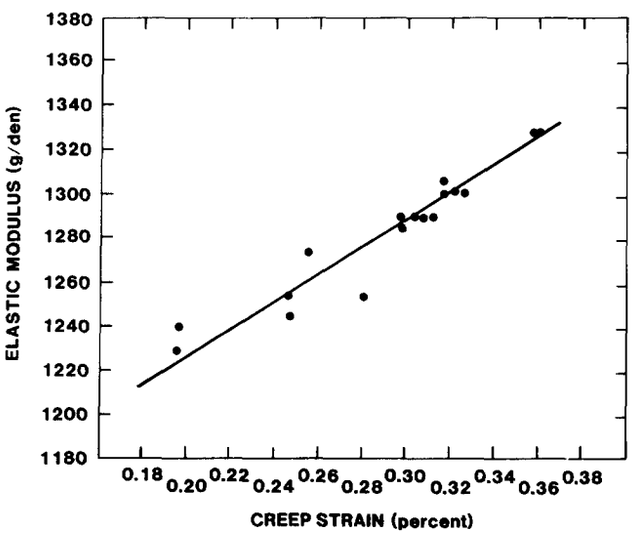

Figure 12 Elastic modulus measured during creep of a Kevlar 29 fibre at room temperature

Northolt and van Aartsen[27] have considered the relationship between deformation of the PPTA fibres and the molecular structure or morphology. They concluded that for a large part of the tensile stress–strain curve the macroscopic strain is brought about by elongation of the crystal lattice through valence angle deformation and bond stretching of the polymer chain. They related the macroscopic compliance, S_{zz}, of a uniaxially symmetric specimen to the crystallite elastic modulus, e_3, and the angle (or average angles) between the symmetry axis of the crystallite (the subscript 3 indicates the direction along the crystallite axis) and the fibre axis (the subscript z denotes the direction along the fibre axis) as

$$S_{zz}=\frac{1}{e_3}+A\langle\sin^2\phi\rangle+B\langle\sin^4\phi\rangle \qquad (4)$$

where A and B are constants involving crystallite elastic moduli e_1, e_3, shear modulus g, and Poisson's ratio v. In a later study, Northolt[28] summarized the fibre structure as being built-up of parallel aligned fibrils in which crystallites having a narrow orientation distribution relative to the fibre axis are linked end to end. Northolt models the strain as originating from the elastic extension of the polymer chain and from rotation of the chain or crystallite axis toward the fibre axis. The rotation is described as consisting of a reversible (elastic) and irreversible (plastic) contribution which accounts for the residual strain observed on unloading an unbroken fibre. The second tensile loading of a fibre is assumed to comprise elastic extension and rotation of the crystallites. Northolt[28] takes the bending force constant of the hydrogen bonds between adjacent chains into consideration in his calculation of the elastic modulus. In addition, he notes a possible significance of the hydrogen bonds for the rotation of the crystallites in that the relative displacement of the crystallites may be controlled by the hydrogen bonds between chains.

Penn and Milanovich[39] compared Raman spectra of Kevlar 49 fibres unstressed and as a function of stress. They did not see frequency shifts which indicates that only minimal stretching or bending of the bonds takes place. They point out that it is difficult to explain the unit cell elongation described by Northolt and van Aartsen[27] in the absence of frequency shifts. They do note that only small amide bond angle changes are required to permit unit cell elongation and this may not cause Raman frequency shifts detectable with their instrumentation. They did see amplitude and depolarization ratio changes with stress and these were interpreted as due to an improved alignment of the crystallites.

CREEP

The stress–strain behaviour described above suggest the possibility that a crystallite rotation process can contribute to fibre creep. The importance of crystallite rotation during creep will be demonstrated in this section. A model

to describe the rotation process will be developed based on experimental observations and published details of fibre structure and morphology. The creep behaviour observed in this study will be discussed in terms of this model. Finally, some alternative creep mechanisms will be considered.

Crystallite rotation

As a starting point, possible mechanisms for crystallite rotation are described. *Figure 13* illustrates two ways in which a pair of crystals can rotate from angle β_0 to angle β_1 with respect to the fibre axis. In case (a) the lattice deforms elastically and valence angles change. This is illustrated schematically as a change in angle α_0 to α_1, so that the crystallites rotate to angle β_1 with respect to the fibre axis without displacement at the interface. Northolt and van Aartsen[27] showed this process, along with elongation of the crystal lattice, contributed to the tensile stress–strain deformation. No change in stress takes place during creep so this elastic deformation cannot contribute to time dependent deformation.

The other crystallite rotation mechanism shown in *Figure 13* is a case where the crystallographic lattice dimensions or angles do not change. Instead, rotation is accomplished by shear at the crystallite interface. These two crystallite rotation modes incorporate the concepts described by Northolt[28] with regard to tensile deformation of PPTA fibres. In actual fibres the crystallites will be distributed over a range of angles and voids or oriented noncrystalline material may play a role in accommodating the crystallite rotation. Voids will be discussed later.

The present results have shown that the fibre modulus increases during a creep test. Data in the DuPont patent[40] shows the fibre modulus is related to the average angle of inclination of the crystallites with respect to the fibre axis, as has the work of Northolt and van Aartsen[27]. These observations, taken with the experimental results of this study, indicate that the crystallite orientation is changing with time during creep by a rotation mechanism. As described, above the rotation must be accomplished by a process involving shear at the intercrystalline boundaries, i.e., by a rigid rotation of the crystallites. The strain accompanying a rigid body rotation from the angle ϕ_0 to ϕ is given by

$$E_r = \frac{\cos\phi - \cos\phi_0}{\cos\phi_0} \tag{5}$$

and the relative importance of this mechanism to the creep deformation can be judged by the amount of creep strain that it can contribute.

The amount of strain due to the crystallite rotation during creep was estimated by using a modulus measured early in the creep test and another obtained after a known amount of creep had occurred to calculate the orientation angles before and after this creep. Two methods or relating modulus to orientation angle were used.

(a) The relationship reported by Northolt[28]

$$S_{zz} = \frac{1}{e_3} + A\langle \sin^2\phi \rangle \tag{6}$$

with $e_3 = 240$ GN/m and $A = 0.26$ m/GN, the values he obtained for his PPTA fibres using sonic modulus measurements.

(b) A linear relationship

$$E = (2450 - 150\,\phi)\ \text{g/den} \tag{7}$$

was obtained from the modulus *versus* orientation angle data reported in the DuPont patent[40] using a limited range of orientation angles (in degrees) appropriate for the present analysis. The change in orientation angle was related to the amount of strain using equation (5) and this calculated strain was compared with that measured experimentally between the two modulus measurements. The results are summarized in *Table 4*. Those obtained using the sonic modulus vs. orientation angle relationship reported by Northolt gave calculated strains that were 25–95% of the measured strain. Using the data from the DuPont patent, the calculated values were 95–180% times the measured strain. No direct relationship has been established between sonic modulus and quasi-static modulus for Kevlar but Northolt has noted that the initial slope of a tensile unloading curve has a value close to the dynamic modulus at that point. In this sense the sonic modulus should be a good comparison with the modulus measurements made during creep.

The modulus vs. orientation angle data from Northolt's work, equation (6), fall on the low angle side of the DuPont data band so it is not surprising that Northolt's relationship results in less strain than that calculated using the DuPont data. The DuPont data exhibit considerable scatter and do not extend to the values of moduli obtained in the creep experiments. Considering the uncertainties in the comparison, the agreement is generally good and indicates that the crystallite rotation mechanism could account for all of the creep strain. In order to further quantify the amount of strain produced by the rotation process, the orientation measurements will have to be made on the same set of fibres used for creep testing.

Crystallite rotation mechanism

The proposed mechanism of crystallite rotation is as follows: rotation is accomplished by shear displacement

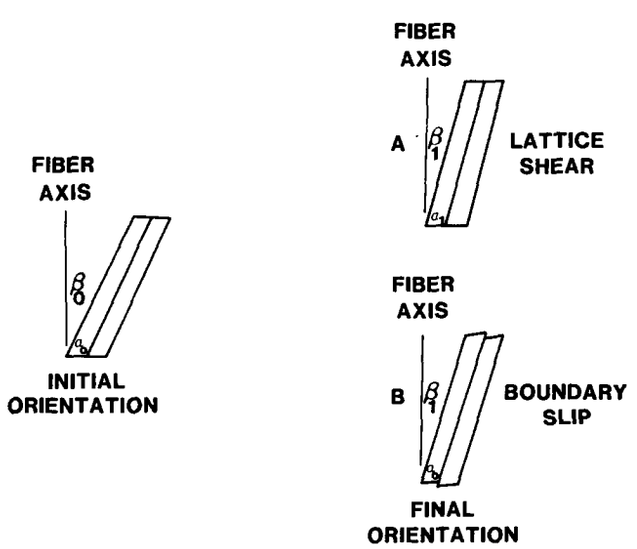

Figure 13 Idealized rotation of two crystallites from orientation β_0 with the fibre axis to orientation β_1. The rotation in (A) is accomplished by lattice deformation (a change in valence bond angle results in lattice constants changing, e.g., from a_0 to a_1). In (B) the crystallite bond angles do not change and the rotation occurs by boundary motion

Table 4 Modulus change during creep

	Modulus g/den		Measured strain	Calculated strain	
	Early in creep	Late in creep		Northolt data	Du Pont data
Kevlar 49	1342	1415	0.0006	0.00012	0.00107
Kevlar 49	1328	1398	0.0006	0.00057	0.00103
Kevlar 49	1263	1330	0.00045	0.00012	0.00105
Kevlar 29	1223	1319	0.0016	0.0009	0.00154
Kevlar 29	1254	1352	0.0013	0.0009	0.0019
Kevlar 29 (2nd loading)	1202	1307	0.0015	0.0010	0.0017

at the crystallite boundaries. The amount and rate of boundary shear is controlled by the time dependent motion of hydrogen and van der Waals bonds in the crystallite boundaries. Details of this mechanism are developed in the following sections. Published details concerning fibre morphology and the experimental results are used as a basis for the model.

Crystallite sizes and boundary structure. Dobb *et al.*[41] report the lattice spacing and apparent crystallite sizes for PRD49, Kevlar 49 and Kevlar fibres as being in the range 3.6 to 8.5 nm based on (110) and (200) X-ray reflections. They also compare the crystallite sizes normal to (110) as measured by WAXS, WAED, and TEM and report values in the range 3.2 to 8.5 nm, depending on the fibre type. Northolt and van Aartsen[27] report that X-ray equatorial reflections of PPTA show profile widths corresponding to crystallite sizes of ~5 nm. Ballou[42] reports two crystallite sizes have been calculated corresponding to directions normal to (020) and (110). These are (a) slightly different, more so for the larger crystallites, (b) not consistent in which they are larger, and (c) in the range from 2 to 14 nm. Hindeleh and Hoseman[43] have compared crystallite size distributions obtained from X-ray data using the theory of paracrystallinity with experimental data reported by Dobb *et al.*[41] and found them in excellent agreement.

There are also suggestions of a fibrillar structure that involves a more macroscopic aggregate of crystallites. Avakian *et al.*[44] have reported, based on electron micrographs of etched fibres, that the fibres consist of 500–700 nm diameter fibrils oriented axially. These authors suggest that in the intact fibre the fibrils probably are held together by tie points, i.e., bundles of molecules which wander from one fibril to an adjacent one.

From the data cited above on the crystallite sizes, it can be concluded that in a 12 μm diameter Kevlar fibre there will be on the order of 1000 to 1500 crystallites across the fibre diameter. This provides a large crystallite boundary area within each fibre so that crystallite rotation can occur on a relatively fine scale with respect to the fibre size.

Interchain bonding in the crystallites consists of hydrogen bonding in the (100) planes with van der Waals forces operating in the other directions[45]. The bonding at intercrystallite boundaries will differ from that within the crystallites since the boundary itself implies mismatch between the crystallites. The make-up of the boundary will depend on the relative orientation of the crystallites and the orientation of the boundary. As a result, we can conclude that any two crystallites will have some non-uniformity in the intercrystalline bonding across their boundary. The boundaries will therefore be more susceptible to bond rearrangement than the crystallites themselves. Zener[46] has pointed out that, since the surface of one crystal cannot fit into the lattice positions of an adjacent one, the binding across the interface of two crystals may reasonably be expected to have the characteristics associated with amorphous materials. A similar argument for lattice mismatch at the boundaries follows from the concept of paracrystallinity. Northolt and van Aartsen[27] have shown X-ray data consistent with the paracrystalline theory and report a distortion parameter of the second kind of 1.7%. Avakian *et al.*[44] have indicated values of 2.0 to 2.5%. Hindeleh and Hoseman[43] point out that boundaries arise in growing paracrystals when distortions at the boundary netplanes reach the point where binding angles of the atoms are overstrained and the netplane breaks.

Time dependent bond motion. The apparent activation energies we obtained for PRD 49 fibre creep were in the range 1.5 to 4.4 kcal mol^{-1} depending on the stress. The value at 10 g (*Figure 9*) was 1.6 kcal mol^{-1}. These activation energies are consistent with the values of 3–7 kcal mol^{-1} for the dissociation energy of hydrogen bonds reported by Rosen[47] and 1–10 kcal mol^{-1} for the activation energy for hydrogen bonds reported by Miller[48]. Yano *et al.*[49] have measured an apparent activation energy of 2.6 kcal mol^{-1} for hydrogen bonding from dynamic mechanical measurements on amorphous cellulose. Mark[50] indicates that the energies required to open hydrogen and van der Waals bonds are between 1 and 5 kcal mol^{-1}, and that hydrogen bonds have a dissociation energy of 5 kcal mol^{-1} and a range of action of about 2.8 Å. The low temperature dependence for creep is consistent with the activation energies expected for hydrogen (or possibly van der Waals bonding) indicating that a mechanism involving intercrystalline bonds can control the creep process.

Mechanisms involving hydrogen bonds have been cited as important in other polymer models. Gordon[51] has examined the anamalous glass transition behaviour in nylons and explained his results based on breakage and time dependent reformation of hydrogen bonds. Since hydrogen bonding sites occur only at intervals along the chain, there are steric factors (problems in matching up potential hydrogen bonding sites) which hinder the formation of a network and explain the time dependence of the transition. Kollross and Owen[52] have interpreted changes in modulus in oriented nylon-12 due to ageing as being a direct result of recombination of hydrogen bonds in the amorphous regions of the semicrystalline polymer. Brunette *et al*[53] have examined hydrogen bond properties in model polyurethanes and suggest that annealing results in an increase in the uniformity of hydrogen bonds. Gilman *et al.*[54] have observed that chain orientation improves during tensile deformation of nylon-6 fibres.

They suggest that this occurs by shear of hydrogen bonded planes and report the change in angle is on the order of 2 to 3 degrees. Hearle and Vaughn[55] discuss the mechanical properties of nylon and suggest that a network of hydrogen bonds is in a state of dynamic equilibrium. They point out that a hydrogen bonded network must be regarded as easily broken by moisture absorption, by rise in temperature, by stress and even (slowly) by thermal fluctuations at room temperature. Under stress, continuing extension will occur as crosslinks slowly break, allow movement, and reform. When stress is removed there will be a slow recovery for the same reason. Consequently nylon will demonstrate appreciable primary creep. Hearle[56] has also shown dynamic mechanical property data for nylon-6 that indicates a major transition due to hydrogen bond crosslinks between 50°C and 150°C.

The difference between the above instances in which time dependent hydrogen bond motion have been cited for polymers and the present situation is that in this case the bond motion is suggested to be in the crystallite boundaries.

Boundary creep and delayed elasticity. Grain boundary sliding contributes to creep of metals; however, in this case the deformation is non-recoverable and normally is not the dominant creep mechanism. There are relatively few cases in which recoverable creep has been associated with grain boundary deformation. One example is that of ice. Simha[57] has shown that the delayed elastic response of ice is grain size dependent. No atomic mechanism for boundary sliding in ice was presented, but ice is an example of a hydrogen bonded structure[58].

In the case of Kevlar fibre creep the recoverable aspect of the creep indicates that delayed elasticity must be considered rather than plastic deformation. Delayed elasticity is characteristic of a disorderly molecular arrangement[59,60] in glassy (amorphous) materials or of disordered regions such as grain boundaries in otherwise crystalline materials. Delayed elasticity does not involve dislocation motion. It has been explained as the thermally activated relaxation of molecular species under the application of an applied stress. It occurs when the mobile species retain their identity and the only change they can undergo is to switch from one to another of their few stable positions. The mobile species are surrounded by an elastic matrix too stable to be rearranged. When the force is removed, the groups return to their former equilibrium distribution and reverse creep (recovery) is obtained. When thermal movement is so intense that the mobile groups cover a large fraction of the volume of the material (so they are no longer surrounded by a virtually rigid matrix) viscous creep will be obtained.

The concepts of delayed elasticity can be applied to the boundary deformation of PPTA fibres with the molecular groups or mobile species defined as hydrogen or van der Waals bonds. Because of the mismatch at the boundaries, there will be a broad distribution of hydrogen and van der Waals bond distances and bond directions. Vitek *et al.*[61] have indicated that in metals the atomic structure of a grain boundary is not unique. An extensive multiplicity of structures can be expected in general boundaries and the energies of different structures are very similar. Such a situation is also possible in the case of intercrystalline boundaries in polymers. The applied stress will give preference to some of the boundary configurations and produce a shear strain as described above. Relatively small scale bond motion is required to produce the small crystallite rotations concluded to take place during creep. A 0.5 degree change in orientation of two adjacent 5×25 nm crystallites requires a 0.04 nm displacement along the 25 nm boundary. The distance between hydrogen bond sites along the polymer chain will be fixed at about 0.6 nm by the PPTA crystal lattice dimensions. The distribution of potential bond sites will depend on the orientation of the two crystallites including their relative displacement along the c-axis. In any event, the 0.04 nm displacement is small compared to the axial or c-axis component of the hydrogen bond spacing.

The strain predicted by the delayed elasticity model is that for the crystallite boundary displacement. It will lead to an angular rotation of the crystallites by a relationship of the form

$$\phi = \phi_0 - \tan^{-1}\frac{\gamma}{d} \tag{8}$$

where γ is the average boundary creep shear strain, d the average crystallite diameter, and ϕ and ϕ_0 are the average angles of the crystallites with respect to the fibre axis. The fibre creep strain is then found from the change in crystallite rotation using equation (5).

Creep time law. Cottrell[62] has pointed out that the observations of similar time laws among radically different solids must mean that the shape of the creep curves are largely independent of the precise atomic processes by which the movements are accomplished. The magnitudes of the coefficients in the time law will be determined by the specific mechanisms producing the deformation.

Argon[63] has investigated the kinetics of delayed elasticity in inorganic glasses where the total number of loose sites is assumed constant. Two shapes of the activation energy spectrum were considered; a narrow one with a single dominant activation energy, and one in which the activation energy spectrum is broad and does not vary rapidly over a wide range of activation energy. In the first case a creep time law of the form

$$\gamma = a\{1 - r^{-bt}\} \tag{9}$$

was obtained. The second case led to a logarithmic time law,

$$\gamma = aL_n t + b \tag{10}$$

As discussed above, the polycrystalline structure of Kevlar fibres results in a range of intercrystalline bond distances and angles in the boundaries. This indicates the likelihood of a borad distribution of activation energies, an argument used by Dinsmore and Statton[64] in their model of as-drawn nylon-6,6 fibres. This corresponds to the condition that Argon[63] showed would lead to a logarithmic creep curve. Argon's expression also indicated a linear increase in creep rate with stress because the shear stresses he considered are small in comparison with the shear modulus. Orowan[60] has pointed out that in polymers the product of the activation volume and the applied stress may be of the order of kT and a much stronger dependence of the strain rate on stress will be obtained.

As pointed out in the experimental results section, the overall dependence of the creep rate on stress has not been completely defined. For the present study the main

conclusion is that the data is consistent with the general aspects of the delayed elasticity theory. For a more quantitative treatment more information concerning the activation energy spectrum will be required, along with a more complete definition of the stress dependence of the creep parameters.

Morphological parameters influencing creep. The parameters in the model which can influence the creep are the initial crystallite orientation (ϕ_0 in equation (5)), the crystallite diameter (d in equation (8)) and the parameters in the time law expression for boundary creep. In the logarithmic expression derived by Argon[63] these would be the number of mobile sites (a fraction of the hydrogen bonds in our interpretation) and the activation volume.

There is some data that will allow relative contribution to the difference in creep between Kevlar 29 and 49 to be evaluated. For the range of initial crystallite orientations present in the Kevlar fibres, the difference in initial orientation will have a negligible influence on the creep behaviour. (For a given change in crystallite orientation, the denominator in equation (5) changes less than 4% when the initial orientation changes from 15 to 5 degrees.) Dobb *et al.*[65] report the crystallite diameter for Kevlar 49 fibres to be about 1.35 times those for Kevlar. If the crystallite diameter for Kevlar is about the same as for Kevlar 29 and does not vary significantly from lot to lot of fibre, these values can be taken as representative of the fibres used in this study. This difference in crystallite diameter would only account for a small part of the difference in creep rate between Kevlar 29 and 49. The small contributions due to initial orientation and to differences in crystallite diameter for this model suggest that a large portion of the factor of three difference in creep between Kevlar 29 and Kevlar 49 is due to differences in boundary creep. Magat[66] indicates an improved perfection in lateral order of polymer chains resulting from the elevated temperature heat treatment used to increase the modulus of the as-spun fibres. This would indicate a decrease in the number of mobile sites and may be the major factor influencing the difference in creep between the different fibre types.

Non-shear boundary displacements. Rotation was described above for the case of two crystallites inclined at the same angle. In the extreme opposite case the adjacent crystallites could be oriented at $+\beta_0$ and $-\beta_0$, for example. In this case rotation requires adjustments between the crystallites. Dobb *et al.*[65] report diffuse low-angle X-ray scattering which may be due to either the presence of microvoids or regions of markedly different molecular packing in the fibres. Their X-ray observations were interpreted as due to voids approximately 6 nm wide by about 25 nm long in both Kevlar 29 and Kevlar 49 fibres. Their electron microscope data also support this interpretation and indicate the microvoids are rod-shaped with their long axis almost parallel to the fibre axis. In another report[46] they report that data from fragmented sheets does not show evidence for voids, implying they are probably located in planes parallel to the sheets.

In the case where the intercrystalline regions between oppositely oriented crystallites are voids, rotation can proceed by a change in the void size or by a void shape change. If voids are not present, either the crystallites must impinge or the intercrystallite regions must contain amorphous or oriented amorphous material. In this case the relative crystallite motion will result in pressure gradients in the boundary regions since the crystallites themselves are assumed not to be deforming. These pressure gradients should result in either (a) void formation or (b) material flow. These processes are analogous to those reported[67] in the case of creep in silicon nitride due to relative grain motion accompanied by grain boundary phase flow and cavitation. Avakian *et al.*[44] state that the fibres are fully crystalline with a very small fraction of randomly oriented crystalline material and that no amorphous material has been detected. Randomly oriented crystalline material could be present but without more information further discussion is not warranted. Note, however, that none of these possibilities preclude the existence of the rotation mechanism.

Rotation accommodation along the fibre axis. For crystallites to reorient with respect to the fibre axis by rigid body rotation governed by transverse boundary shear there must be structural adjustments at the crystallite boundaries normal to the fibre axis. Crystallite lengths from (004) and (006) X-ray reflections have been reported by Dobb *et al.*[41] for PRD 49, Kevlar 49, and Kevlar to be in the range 6 to 18 nm. Northolt[28] reported a crystallite size along the fibre axis of about 25 nm. He concluded that the fibre structure was built-up of parallel aligned fibrils in which the crystallites have a narrow orientation distribution relative to the fibre axis and are linked end to end. Avakian *et al.*[44] describe the structure along the fibre axis as a high proportion of extended chains passing through periodic defect layers. They indicate that X-ray small-angle scattering data show a defect spacing or a long period of 20–30 nm that is smaller than the correlation length which is over 80 nm. This is the same situation as reported by Gibson, Davies and Ward[68] for ultra high modulus polyethylene. Northolt and van Aartsen[27] have noted that a small-angle pattern resembling a two point pattern has not been observed in PPTA up to a resolution of 250 A. Tashiro *et al.*[69] conclude that the extended chain structure or oriented amorphous structure may be reasonably considered for Kevlar. Slutsker *et al.*[70] report small-angle X-ray scattering from PPTA fibres and a long period of 19 nm. They conclude that the long periods in PPTA fibres are made up of alternating more dense, more ordered, crystalline regions and less dense, less ordered intercrystallite layers. They present a model for the intercrystallite layers and suggest that sections of the tie molecules in these regions can be expected to be of different length so that some of them are bent while the others are extended. However, they point out that the elastic modulus of bent molecules in aromatic polymers does not differe stongly from that of the extended molecules. Thus both extended and bent chains are load bearing. From acoustic measurements they conclude that for PPTA an estimate of the fraction of load bearing chains in crystallites per unit cross section to be 0.5. They estimate this to be a lower bound.

All the above investigators seem to be in general agreement that there are periodic boundaries along the fibre axis and a large number of the polymer molecules traverse the boundaries and provide continuity along the fibre axis. In terms of the present model, the crystallite rotation can be accommodated by the boundaries deforming as hinges with a strain gradient produced in the polymer chains crossing the boundary depending on their

position with respect to the pivot. The maximum strain will occur in the polymers farthest away from the pivot and will be determined by the amount of rotation, the length to diameter ratio of the crystallites, and the amount of slack or bending originally present in the molecules at the boundary. Northolt and van Aartsen[27] have observed a decrease in X-ray profile width and an increase in intensity when samples are examined under load. This was interpreted as caused by better alignment and increased perfection of the crystallites.

The amounts of strain observed during creep correspond to about 0.5 degrees of crystallite rotation. If two aligned crystallites are rotated, a simple geometric calculation predicts the amount of strain required if deformation is limited to the boundary. Assuming the crystallites have a length to diameter ratio of 5 (that expected base on the data reported above[28,41]), and that all the deformation is localized into a length of polymer equal to one unit cell, then the unit cell most remote from the pivot region will be strained about 3%. If these boundaries deform during creep their extension may contribute to the driving force for creep recovery.

Irreversible creep on initial loading. The irreversible portion of the initial creep appears to be related to the process leading to the residual strain obtained at the end of the first load unload cycle in a repeated loading test. Northolt[28] has suggested that relaxation processes accompany the rotation of crystallites and these result in an apparently lower force constant even during the second loading. In terms of the crystallite rotation mechanism one possible interpretation would be a decrease in the number of mobile sites during initial creep. Fewer mobile sites would reduce the recovery rate on unloading and also it would lead to a lower initial rate of recovery compared with the lower creep rate on the second loading.

Other creep mechanisms

The crystallite rotation mechanism seems to account for the observed experimental observations. However, it is appropriate to consider some other possibilities.

Internal stress. Relaxation of internal stress resulting from fibre fabrication could lead to time dependent strain. This would most likely not explain creep or the creep observed in repeated loading cycles. There is also some evidence that little internal stress is present in Kevlar fibres. Allen *et al.*[71] studied Benzobisthiazole (PBT) fibres and compared some of the data to that obtained on Kevlar 49. Plastic deformation was observed in as-spun PBT fibres and was explained on the basis of internal stresses. Plastic deformation was not observed in heat treated PBT fibres and the similarity between the stress–strain curves for heat treated PBT and Kevlar fibres in addition to the similarity in structure was cited as evidence that internal stresses were not present in the Kevlar. In a further test, PBT, heat treated PBT, and Kevlar were placed in a laser beam to induce damage in a region near the fibre surface. (This should relieve stresses locally and produce bending if residual stresses are present.) Bending was observed in the PBT but not in the heat treated PBT and Kevlar fibres. This was cited as further evidence that residual stresses are not present in the Kevlar.

Molecular rearrangement. Tashiro *et al.*[69] investigated the relationship between the elastic moduli and molecular structure for some aromatic polyamides. They concluded that the all-*trans* conformation in Kevlar cannot transform easily to cis or gauche forms because of the high barriers of the virtual bonds and also of the amide bonds. Tadokoro[72] has summarized these and other studies of PPTA crystallite deformation and points out that because Kevlar has a *TTTT* (fully extended all-*trans*) type molecular conformation, the changes in the internal rotational angles cannot contribute to the elongation of the molecular chain. The elongation can arise only by changes in the bond angles and bond lengths. There is no indication from these studies that time dependent elastic processes within individual crystallites could lead to the observed creep behaviour. The rate of creep is higher in Kevlar 29 than in Kevlar 49, yet the crystal structure is the same in both cases. The only difference is in crystallite morphology and orientation. This argues against any mechanism of creep involving crystal lattice deformation.

Supramolecular (pleat) structure. Dobb *et al*[73] have observed a supramolecular structure in Kevlar and Kevlar 49 fibres. They showed that the supramolecular architecture of these fibres consists of a system of sheets regularly pleated along their long axes and arranged radially. They did not observe this structure in PRD 49 fibres. Dobb points out that near-meridional reflections cannot be completely accounted for by Northolt's[74] unit cell. One possible explanation cited by Dobb *et al.*[73] was that pleating of the hydrogen bonded sheets introduces a different crystalline structure by displacing the sheets relative to each other as they bend to form the pleats. Simmins and Hearle[75] used optical microscopic techniques to study Kevlar 29 and saw bands similar to one type reported by Dobb *et al*[73]. Ballou[42] also indicates periodic structural variation with a period on the order of 1 μm. This was interpreted as being caused by longitudinal bending of aggregates of polymer chains through small angles on the order of 5 degrees. At present the pleated structure has not been directly related to any aspect of the mechanical behaviour of the fibres. Ballou[42] does note that PPTA fibres can approach perfect orientation when loaded to failure in tension, indicating that periodic bending in the structure can be pulled out by stress. However, some reservation was cited for the extent of perfection in orientation that might be obtained[3].

The PRD 49-III fibres tested in this study crept faster than the Kevlar 49 fibres. If a pleat structure is present in the Kevlar 49 fibres but not in our PRD 49-III fibres, it would be expected that the Kevlar 49 might creep faster contrary to our experimental observations. Our PRD 49-III fibres had a lower modulus than the Kevlar 49 fibres we investigated, but the reverse situation was noted by Dobb *et al.*[73] for the PRD49 and Kevlar 49 used in this study. The relative ranking of the three fibres used in this study in terms of creep rate was consistent with the ranking in elastic modulus. At present the pleat structure, if it is present in Kevlar but not the PRD 49-III fibres, does not appear to correlate with any trends in the creep data.

Void and crack formation or growth. As described above, voids and some large cracks have been observed in Kevlar fibres. The specific relationship between the defects present in the fibres and their mechanical properties has not been established. It is possible that voids play a role in the crystallite rotation mechanism as described above. The tensile breaking strength of PRD 49-III fibres decreases as

the specimen gauge length is increased[76] and this is consistent with failure initiating at flaws in the structure.

Venkateswaran and Hasselman[77] have considered some mechanisms for elastic creep due to time-dependent changes in elastic properties. They consider voids as one case and crack growth as another. They point out that cavities in many materials undergoing creep are a well-known phenomenon and that cavities will reduce the elastic moduli. In other materials crack formation and growth can lead to elastic creep. Any decrease in modulus due to void growth during creep in the Kevlar fibres would be masked by the modulus increase caused by crystallite rotation. The above considerations fail to provide an alternate creep mechanism that would be consistent with the experimental results. The crystallite rotation mechanism can account for the magnitude of the creep strain and provides a qualitative description of the other features of Kevlar fibre creep.

CONCLUSIONS

(1) Creep in Kevlar 29, Kevlar 49, and PRD 49-III fibres could be adequately described using a logarithmic time law.

(2) The creep rate for a given fibre at any time increases with stress. For a given stress the creep rate for the three fibres investigated was higher for Kevlar 29, intermediate for PRD 49-III, and lowest for Kevlar 49. This is the same ranking as obtained for the tensile moduli.

(3) The creep strain recovered with time according to a logarithmic time law. The creep rate after initial loading was higher than the rate observed if the specimen was crept, allowed to recover, and then reloaded.

(4) The elastic modulus was measured during a creep test and was found to increase with time. This was interpreted as resulting from crystallite rotation during creep.

(5) The strain expected from crystallite rotation was estimated and found to approximate that obtained experimentally.

(6) The measured apparent activation energy for creep was found to compare favourably with values associated with hydrogen bonding. The data supports a model in which the combined action of stress and thermal activation cause rearrangement of hydrogen bonds in the intercrystallite boundaries permitting boundary shear and crystallite rotation.

(7) The logarithmic creep behaviour can be explained based on the theory of delayed elasticity for the case where a broad distribution of activation energies is present.

ACKNOWLEDGEMENTS

The author wishes to acknowledge the assistance of Mr L. E. Hermesmeyer, Mr K. D. Boultinghouse and Mr L. Orear in carrying out the experimental aspects of this work. Helpful discussions with Drs W. E. Warren, E. D. Reedy, Jr., S. C. Kunz and F. P. Gerstle, Jr., are greatly appreciated.

REFERENCES

1 Preston, J. *Polym. Eng. Sci.* 1975, **15(3)**, 199
2 Preston, J. 'Synthesis of Ultra-High Strength/High Modulus Fibers from Wholly Aromatic Polymers, in Ultra-High Modulus Polymers', (Eds. A. Ciferri and I. M. Ward), Applied Science Pub., London, 1977, p. 155
3 Schaerfgen, J. R., Bair, T. I., Ballou, J. W., Kwolek, S. L., Morgan, P. W., Panar, M. and Zimmerman, J. in 'Ultra-High Modulus Polymers', (Eds. A. Ciferri and I. M. Ward), Applied Science Pub., London, (1977), p. 173
4 Black, W. B. and Preston, J. (Eds.) 'High-Modulus Wholly Aromatic Fibers', Marcel Dekker, New York (1973)
5 Berry, G. C. and Srogg, C. E. (Eds.) *J. Polym. Sci.* 1978, **65**, 222
6 Morgan, P. W. *Macromolecules* 1977, **10**, 1381
7 Kwolek, S. L., Morgan, P. W., Schaefgen, J. R. and Gulrich, L. W. *Macromolecules* 1977, **10**, 1390
8 Blair, T. I., Morgan, P. W. and Killian, F. L. *Macromolecules* 1977, **10**, 1396
9 Schaefgen, J. R. in 'The Strength and Stiffness of Polymers', (Eds. A. E. Zachariades and R. S. Porter), M. Dekker, New York, 1983, p. 327
10 Blumstein, A. (Ed.) 'Liquid Crystalline Order in Polymers', Academic Press, New York (1978)
11 Carter, G. B. and Schenk, T. T. J. in 'Structure and Properties of Oriented Polymers', (Ed. I. M. Ward), Halstead, New York, 1975, p. 454
12 Black, W. B. in 'Flow Induced Crystallization', (Ed. R. L. Miller), Gordon and Breach, New York, 1979, p. 245
13 Black, W. B. *Ann. Rev. Mater. Sci.* 1980, **10**, 311
14 Black, W. B. *Macromol. Sci.–Chem.* 1973, **A7(1)**, 3
15 Chiao, C. C. and Chiao, T. T. 'Aramid Fibers and Composites', Lawrence Livermore National Laboratory Technical Report UCRL-80400 (1977)
16 Konopasek, L. and Hearle, J. W. S. *J. Appl. Polym. Sci.* 1977, **21**, 2791
17 Hearle, J. W. S. and Wong, B. S. *J. Mater. Sci.* 1977, **12**, 2447
18 Bunsell, A. R. *J. Mater. Sci.* 1975, **10**, 1300
19 Dobb, M. G., Johnson, D. J. and Saville, B. P. *Polymer* 1981, **22**, 43
20 Greenwood, J. G. and Rose, P. G. *J. Mater. Sci.* 1974, **9**, 1809
21 Wilfong, R. E. and Zimmerman, J. *J. Appl. Polym. Sci., Appl. Polym. Symp.* 1977, **31**, 1
22 Chiao, C. C., Sherry, R. J. and Chiao, T. T. *Composites* 1976, **7**, 107
23 Morgan, R. J., Mones, E. T., Steele, W. J. and Deutscher, S. B. 'The Failure Modes and Durability of Kevlar/Epoxy Composites', Proceedings of the 12th Nat. SAMPE Technical Conference, 7–9 Oct. 1980, Seattle, WA, USA
24 Hahn, H. T. and Gates, T. L. 'Effect of Storage Time on Tensile Strength of Kevlar 49/Epoxy Strands', Lawrence Livermore National Laboratory Technical Report, UCRL-82698 (1979)
25 Morgan, R. J., Mones, E. T., Steele, W. J. and Deutscher, S. B. 'The Structure and Property Relationships of Poly(*p*-Phenylene Terephthalamide) Fibers', Lawrence Livermore National Laboratory Technical Report UCRL 85744 (1981)
26 Morgan, R. J., Pruneda, C. O. and Steele, W. J. *J. Polym. Sci.* 1983, **21**, 1573
27 Northolt, M. G. and van Aartsen, J. J. *J. Polym. Sci., Polym. Symp. Edn.* 1977, **58**, 283
28 Northolt, M. G. *Polymer* 1980, **21**, 1199
29 Chiao, T. T., Wells, J. E., Moore, R. L. and Hamstad, M. A. 'Stress–Rupture Behavior of Strands of an Organic Fiber/Epoxy Matrix, in Composite Materials: Testing and Design', American Society For Testing and Materials, Philadelphia, PA, ASTM STP-546 (1974), p. 209
30 Penn, L. 'Stress–Rupture Life and Strength Retention of an Aramid Fiber/Epoxy Composite under Accelerating Conditions, Proceedings of Failure Modes and Processing of Composites IV', The Composite Materials Committees of the Metallurgical Society of AIME and of The American Society of Metals, Chicago, 24–27 Oct. 1977
31 Phoenix, S. L. and Wu, E. M. 'Statistics for the Time Dependent Failure of Kevlar-49/Epoxy Composites: Micromechanical Modeling and Data Interpretation', IUTAM Symposium on Mechanics of Composite Materials, 16–19 Aug. 1982, VIP&SU, Blacksburg, VA
32 Kevlar 49 DP-01 Data Manual, E. I. DuPong & Co., Textile Fibers Department, Wilmington, Delaware 19898
33 Ericksen, R. H. *Composites* 1976, **7**, 189
34 Bott, T. R. and Barker, A. J. *Ind. Eng. Chem.* 1967, **59**, 46
35 Ericksen, R. H. *Fiber Sci. Tech.* 1974, **7**, 173
36 Sturgeon, J. B. 'Fatigue and Creep Testing of Unidirectional Carbon Fiber Reinforced Plastics', Proc. 28th Annual Technical Conference, The Society of the Plastics Industry, Inc. (1973) Sec. 12-B, p. 1
37 Conway, J. B. 'Numerical Methods for Creep and Rupture

Analysis', Gordon and Breach, New York, 1967
38 Ko, F. K. in 'Advances in Composite Materials', (Eds. A. Bunsell *et al.*), Pergamon Press, New York, Vol. 1, p. 719 (1980)
39 Penn, L. and Milanovich, F. *Polymer* 1979, **20**, 31
40 Kwolek, S. L. US Patent 3 671 542 Assigned to the DuPont Co. (1972)
41 Dobb, M. G., Johnson, D. J. and Saville, B. P. *J. Polym. Sci. Polym. Symp. Edn.* 1977, **58**, 237
42 Ballou, J. W. *Polym. Prepr.* 1978, **17**, 1
43 Hindeleh, A. M. and Hosemann, R. *Polymer* 1982, **23**, 1101
44 Avakian, P., Blume, R. 3., Gierke, T. D., Yang, H. H. and Planar, M. *Polym. Prepr.* 1980, **21**(1)
45 Dobb, M. G., Johnson, D. J. and Saville, B. P. *Phil. Trans. Roy. Soc., London* 1979, **A294**, 483
46 Zener, C. 'Elasticity and Anelasticity of Metals', University of Chicago Press, Chicago, 1948
47 Rosen, S. L. 'Fundamental Principles of Polymeric Materials', Barnes and Nobel, New York, 1971
48 Miller, M. L. 'The Structure of Polymers', Reinhold, New York, (1966), p. 169
49 Yano, S. and Hatakeyama, Y. *J. Appl. Polym. Sci.* 1976, **20**, 3221
50 Mark, H. in 'Polymer Science and Materials' (Eds. A. V. Tobolsty and H. F. Mark), Wiley, Interscience, New York (1971)
51 Gordon, G. A. *J. Polym. Sci. A-2* 1971, **9**, 1693
52 Kollross, P. and Owen, A. J. *Polymer* 1982, **23**, 829
53 Brunette, C. M., Hsu, S. L. and MacKnight, W. J. *Polym. Prepr.* 1978, **19**, 1
54 Gilman, T. H., Resetarits, M. R. and Christ, Jr., B. *Polym. Eng. Sci.* 1978, **18**, 477
55 Hearle, J. W. S. and Vaughn, E. A. 'Mechanical Properties of Fibres and Fibre Assemblies in Polymer Science', (Ed. A. D. Jenkins), North-Holland (1972)
56 Hearle, J. W. S. *J. Polym. Sci., C* 1967, **20**, 215
57 Sinha, N. K. *Phil. Mag.* 1979, **40(6)**, 825
58 Nowick, A. S. and Berry, B. S. 'Anelastic Relaxation in Crystalline Solids', Academic Press, New York (1972)
59 Orowan, E. 'Creep in Metals and Polymers', Proceedings of the First National Congress on Applied Mechanics, ASME, New York (1952), p. 453
60 Orowan, E. in 'Mechanical Behavior of Materials', (Eds. F. A. McClintock and A. S. Argon), Addison-Wesley, Reading, MA (1966)
61 Vitek, V., Sutton, A. P., Wang, G. J. and Schwartz, D. *Scripta Met.* 1983, **17**, 183
62 Cottrell, A. H. *J. Mech. Phys. Solids* 1952, **1**, 53
63 Aragon, A. S. *J. Appl. Phys.* 1968, **39**, 4080
64 Dismore, P. F. and Statton, W. O. *J. Polym. Sci., C* 1966, **13**, 133
65 Dobb, M. G., Johnson, D. J., Majeed, A. and Saville, B. P. *Polymer* 1980, **20**, 1284
66 Magat, E. E. *Phil. Trans., Roy. Soc. London* 1980, **A294**, 463
67 Arons, R. M. and Tien, J. K. *J. Mater. Sc8.* 1980, **15**, 2046
68 Gibson, A. G., Davies, G. R. and Ward, I. M. *Polym. Eng. Sci..* 1980, **20**, 941
69 Tashiro, K., Kobayashi, M. and Tadokoro, H. *Macromolecules* 1977, **10**, 413
70 Slutsker, L. I., Utevskii, L. E., Chereiskii, Z. Yu. and Perepelkin, K. E. *J. Polym. Sci., Polym. Symp. Edn.* 1977, **58**, 339
71 Allen, S. R., Filippov, A. F., Farris, R. J. and Thomas, E. L. *J. Appl. Polym. Sci.* 1981, **26**, 291
72 Takokoro, H. 'Structure of Crystalline Polymers', Wiley-Interscience, New York (1979)
73 Dobb, M. G., Johnson, D. J. and Saville, B. P. *J. Polym. Sci.* 1977, **15**, 2201
74 Northolt, M. G. *Eur. Polym. J.* 1974, **10**, 799
75 Simmens, S. C. and Hearle, J. W. S. *J. Polym. Sci.* 1980, **18**, 8710
76 Ericksen, R. H. unpublished research
77 Venkateswaran, A. and Hasselman, D. P. H. *J. Mater. Sci.* 1981, **16**, 1627